Numerical Study of Viscous Dissipation, Suction/Injection Effects and Dufour Number also with Chemical Reaction Impacts of MHD Casson Nanofluid in Convectively Heated Non-Linear Extending Surface

Sanju Jangid[1], *Ruchika Mehta*[1*] *and Devendra Kumar*[2]
[1,1*] *Department of Mathematics and Statistics*,
Manipal University Jaipur, Jaipur(Raj.), India
[2] *Departmentof Mathematics*,
University of Rajasthan, Jaipur(Raj.), India
[1*] *ruchika.mehta*1981@*gmail.com*

January 1, 2022

Abstract

This numerical study looked at the effects of thermophoresis diffusion, Brownian motion parameter influences, and suction/injection influence in a hydromagnetic (MHD) Casson nanofluid in a convectively heated nonlinear extending surface (in 2D). Using similarity transformations, the leading partial differential equations (PDEs) are renewed into a set of ordinary differential equations (ODEs) with suitable boundary conditions, and then numerically resolved using a 4^{th}order Runge-Kutta approach based on the shooting technique and the MATLAB application. Graphs are used to investigate the effects of dimensionless parameters such as local Grashof temperature and concentration parameter, permeability, Joule impact, thermo radiative impression, Dufour and chemical reactive impression on nanoparticle volume fraction profiles, temperature, and movement. Tables and graphs are used to examine other characteristics of importance, such as the skin friction coefficient, heat, and mass transfer in a variety of situations, as well as the relationship between these parameters.

Key words: Casson Nanofluid; MHD; Heat Generation/Absorption, Thermophoresis Diffusion, RK-4^{th} order.

1 Introduction

There are several applications, including the learning of non-Newtonian fluids across an extended sheet, which was completed with extreme kindness. Although the elasticity of non-Newtonian fluid behaviour may be assessed, their fundamental equations are occasionally used to classify the rheological features. The fundamental relations in non-Newtonian fluids are extra difficult because they provide the rheological non-dimensional characteristics. Non-Newtonian fluids include a variation of fluids used in the oil industry, as well as cooling courses for micro-ships, unclosed-flow switching, and multiplex systems.

Because of its applications in paramedical sciences, geo and astrophysics, oil reservoirs, and geothermal engineering, free convective heat transport is a mean-

ingful part of fluid dynamics. The term "thermal radiation" refers to a method of converting internal energy into electromagnetic waves. Thermal radiation and nonlinear thermal radiation are employed in a variety of applications, including space vehicles, paper and glass manufacture, gas turbines, space technologies, and hypersonic combat. The flow model is based on a mix of Tiwari and Das models, as well as the Buongiorno's model.The influence of MHD Casson fluid flow through a convective surface with crossdiffusion, chemical reaction, and nonlinear radiative heat is accounted for using convective and boundary conditions, according to Ramudu et al. [1].Butt et al. [2] assessed the entropy generative impression of a flow traversed by a permeable stretched surface of hydromagnetic Casson nanofluid. Afify [3] addresses Casson nano fluid's work in the presence of viscid dissipative impression on a stretched sheet with slip limits. AlHossainy et al [4] address a SQLM (spectral quasi linearization method) mathematical work for the impact of stress on hydromagneto nanofluid flow with permeability influence in three dimensions. The timedependent nonlinearly convective stream of thin film nano liquid across an inclined stretchable sheet with a magnetic effect was studied by Saeed et al. [5]. The use of this current fractional operator to investigate Newtonian heating impacts for the generalized Casson fluid flow is the focus of Tassaddiq et al. [6] research. In this study, the MHD and porous impacts of such fluids are also taken into account. MHD Casson nanofluid (Ag and Cu water) boundary layer flow and heat transference across a stretched surface through a porous mode were studied by Siddiqui and Shankar [7]. Faraz [8] investigated a mathematical study on an axisymmetric Casson nanofluid flow over a radially stretched sheet with hydromagnetic impact. Hady et al. [9] inspected the radiative effect and heat transmission of a viscid nanofluid across a nonlinear stretched sheet. In the company of porous mode, Mahantha and Shaw [10] proposed a 3dimensional convective Casson fluid flow with convective limits passing through a linear stretched sheet. Vendabai [11] investigate a hydromagnetic boundary layer Casson nanofluid flow passing through an upright exponentially stretched cylinder with transverse magneto impact and heat generating or absorptive impression. Alotaibi et al. [12] investigated the influence of viscid dissipative impact over a convectively intensive nonlinear spreading surface, as well as suction or injection and heat absorption or generation impacts, on a hydromagnetic boundary layer flow of Casson nanofluid flow. Oyelakin et al. [13] studied a flow of timedependent Casson nanofluid across a stretched surface with thermal radiative imprint and slip limiting settings.

Many studies of Newtonian and nonNewtonian fluids have been directed in order to examine the impacts of fluid movements, as well as various types of nanofluid flows across various surfaces. In fresh years, a large number of inspections on the boundary layer flow of Casson nanofluids in a variety of geometries have been carried out. Ullah et al. [14] looked at the effect of thermo radiative, convective limiting circumstances, and heat generation/absorption on a timedependent hydromagnetic mixed connective slip Casson fluid flow, as well as chemically reactive influence, on a nonlinearly stretched sheet in a porous mode. The local fractional linear transport equations (LFLTE) in fractal porous media are studied by Singh et al. [15]. Dwivedi and Singh [16] produced a new finite difference collocation approach that was designed using the Fibonacci polynomial and then used to one super and two sub-diffusion problems with better reliability. Imtiaz et al. [17] examined how a convective Casson nanofluid flow goes through a stretched cylinder and the restrictions that come with it. Eid and Mahny [18] describe a computational study to determine the heatgenerating influence of Sisko nanofluid across a nonlinear stretched sheet with porous mode. Eid [19] investigated a twophase nanofluid flow with hydromagnetic influence, as well as chemical reactive and heat generating effects, across an exponentially stretched sheet. Chemical reaction effects on a convectively heated nonlinear stretched surface of Carreau nanofluid were explored by Eid et al [20].

Eid [21] investigated the chemical reactive effects of H_2O-NPs (nanoparticles) in unsteady and stagnation point flow on a stretched sheet in the soaking porous mode. Mustafa and Khan [22] investigated a Casson model flow over a nonlinear stretched sheet with magneto impacts. Wahiduzzaman et al [23] did a mathematical investigation of hydromagnetic Casson fluid flow in the presence of porous mode passing through a nonisotherm stretched sheet. The Casson nanofluid flow between stretched discs with radiative influence was deliberated by Khan et al [24]. The viscid dissipative impression of hydromagnetic Casson nanofluid passing through permeable stretched sheet was observed by Besthapu and Bandari [25]. Pramanik [26] discusses the thermo radiative and Nusselt number impressions in the presence of a porous mode of nonNewtonian Casson flow passing over an exponentially stretched surface.

The vast range of commercial and manufacturing experiments of flow behaviour across stretched surfaces has attracted numerous writers, including artificial fibres, metallic sheet manufacture, petroleum industries, metal spinning, polymer processing, and so on. Reddy[27] examined the thermal radiative effect and chemically reactive impact of a hydromagnetic Casson fluid flow over an exponentially persuaded permeable stretched surface. Vijayaragavan [28] used a permeable stretched sheet to investigate the heat source or sink effect of timeindependent hydromagnetic Casson fluid flow. Haq et al. [29] examined timedependeny free convection slip flow of secondgrade fluid across an endless hot inclined plate. Lahmar et al. [30] examined the impacts of thermal conductivity and Nusselt number on the squeezing of a timedependent nanofluid by a tending magneto. Nadeem et al. [31] considered a nonNewtonian shear thinning Casson fluid flow with permeability impact passes across a stretchy linear sheet. Mass transference of hydromagnetic Casson fluid with suction and chemical reactive impression was explored by Shehzad et al [32]. Dahab et al. [33] investigated the influence of extending surface over a nonlinearly heated extending surface using hydromagnetic Casson nanofluid flow. Ibrahim et al. [34] conducted a mathematical investigation of a dissipative hydromagnetic mixed convective Casson nanofluid with chemical reactive effect across a nonlinear permeable stretched sheet with heat source impression. Hayat et al. [35] took into account mixed convective stagnation point Casson fluid flow as well as convective constraints. The goal of Puneeth et al. [36] is to figure out what function mixed convection, Brownian motion, and thermophoresis play in the dynamics of a Casson hybrid nanofluid in a bidirectional nonlinear stretching sheet. The heat transfer and entropy of an unstable Casson nanofluid flow, where fluid is positioned across a stretched flat surface flowing nonuniformly, were explored by Jamshed et al. [37]. Over a nonlinear stretched sheet, Shah et al [38] discussed chemically reactive hydromagnetic Casson nanofluid flow with radiation influence and entropy generating impression. Soret or diffusion thermo or thermo difusion effect is described as matter diffusion caused by a gradient of heat, whereas Dufour efect is defined as heat diffusion caused by a gradient of concentration. For excessively big temperature and concentration gradients, these consequences have played a substantial influence. The majority of the time, these two impacts are regarded as secondorder effects. Its uses include contaminant movement in groundwater, chemical reactors, and geosciences. Several academics are drawn to the field of heat flux mass transfer because of its wide range of applications in numerous fields. Fiber optics manufacturing, plastic emulsion, glass cutting, nanoelectronics freezing, catalytic reactors, wire drawing, and improved oil extraction are all examples of Brownian motion effects and thermophoresis in the scientific and technical sphere.

The current study attentions on the Casson nanofluid flow over a nonlinear inclined stretching surface with Buoyancy and Dufour impacts, as a result of the above mentioned literature review and the rising need for nonNewtonian nanofluid

flows in industry and engineering. When compared to Newtonian based nanofluid flow, Casson nanofluid is more useful for cooling and friction-reducing agents. The goal of this research is to show a comprehensive mathematical investigation of the impression of buoyancy force, permeability, joule heating impression, and chemical reactive with heat generative or absorption, suction or blowing impact, and viscid dissipative impression of 2-dimensional hydromagneto Casson fluid flow permits through nonlinear outspreading plate along with CBC (convective boundary conditions) ref [12]. PDEs (dimension form) of existing effort were turned into ODEs with the support of several similarity transformations. The RK4th order process cracked nondimensional ODEs with the help of the shooting procedure. MATLAB software is used to create graphs and tables that highlight the rooted parameter behaviour.

2 Problem Structure:

Deliberate hydromagnetic convective nanofluid flow in the section ($y > 0$) over an exponentially extensible sheet as 2-dimensional incompressible (density is constant) time-independent viscid along with the impact of the viscous dissipative and several non-dimensional parameters. X-axis indicated for surface and y-axis erect to surface. The extensible surface is projected to have a velocity outline of the power law $u_w(x) = ax^n$ where a, n is non-zero constants. Magnetic field is covered with $B(x) = B_0 x^{(n-1/2)}$ and the electric field is zero, but the induced magnetic field is unnoticed by the weak magnetic amount of Reynolds. $T_w(x) = T_\infty + Ax^n$, where A is non-zero secure rate, T_∞ displays the free stream temperature. C_∞ displays the ambient nano-particles concentration. Flow chart of existing work is exposed in [Figure 1].

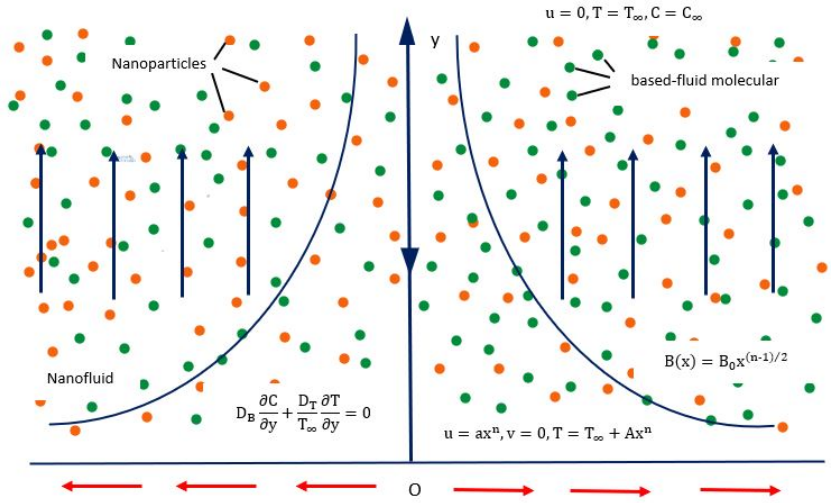

Figure 1: Bodily Modal of recent effort.

The Casson fluid rheological state equation [references [21], [31]] is:

$$\tau_{ij} = \begin{cases} 2(\mu_B + \frac{\tau_y}{\sqrt{2\pi}})e_{ij} & \text{if } \pi > \pi_c \\ 2(\mu_B + \frac{\tau_y}{\sqrt{2\pi}})e_{ij} & \text{if } \pi < \pi_c \ . \end{cases} \tag{1}$$

Where deformation component rate product $\pi = e_{ij}e_{ij}$, where e_{ij} displays the $(i, j)^{th}$ deformation component rate, π is the multiple of the sections of deformation

component rate product, π_c indicates to the non-Newtonian fluid critical rate of this deformation component rate product, μ_B signifies Casson fluid plastic viscosity, τ_y shows yield stress.

Consider the apparatuses of velocity function $V = [u(x,y), v(x,y), 0]$, the temperature function $T = T(x,y)$ and concentration function $C = C(x,y)$. The motion, temperature and the concentration relations in a Casson nanofluid are inscribed as

$$\frac{\partial u}{\partial x} + \frac{\partial v}{\partial y} = 0, \tag{2}$$

$$u\frac{\partial u}{\partial x} + v\frac{\partial v}{\partial y} = \nu(1+\frac{1}{\beta})\frac{\partial^2 u}{\partial y^2} - \frac{\sigma B^2(x)u}{\rho_f} - \frac{\nu}{k'}u + g_0\beta_T(T-T_\infty) + g_0\beta_C(C-C_\infty), \tag{3}$$

$$u\frac{\partial T}{\partial x} + v\frac{\partial T}{\partial y} = \alpha\frac{\partial^2 T}{\partial y^2} + \frac{Q_0}{\rho c_p}(T-T_\infty) + \tau[D_B(\frac{\partial T}{\partial y}\frac{\partial C}{\partial y}) + \frac{D_T}{T\infty}(\frac{\partial T}{\partial y})^2] + \frac{\mu}{\rho c_p}(1+\frac{1}{\beta})(\frac{\partial u}{\partial y})^2$$
$$+ \frac{\sigma B^2(x)u^2}{\rho c_p} - \frac{1}{\rho c_p}\frac{\partial q_r}{\partial y} + \frac{D_B K_T}{c_s c_p}\frac{\partial^2 C}{\partial y^2}, \tag{4}$$

$$u\frac{\partial C}{\partial x} + v\frac{\partial C}{\partial y} = D_B\frac{\partial^2 C}{\partial y^2} + \frac{D_T}{T_\infty}\frac{\partial^2 T}{\partial y^2} - k_1(C - C_\infty). \tag{5}$$

where, u and v show the x-axis and y-axis velocity apparatuses respectively, ν displays the kinematic viscosity, $\beta = \mu_B\frac{\sqrt{2\pi_C}}{\tau_y}$ indicates the Casson fluid parameter, σ displays the conductivity electrical field, ρ indicates the fluid density, the thermophoresis and Brownian diffusions coefficients are direct by D_T, and D_B respectively, Q_0 specifies the dimensional heat source or sink coefficient, α shows the thermal diffusivity, T pointed for temperature,$\tau = \frac{(\rho C)_p}{(\rho C)_f}$ directs the ratio of the effective heat capacity to efficient liquid heat capacity, and C_p indicates the specific heat.

The existing work boundary conditions are specified by

$$u = u_w = ax^n,\ v = v_w,\ T = T_w = T_\infty + Ax^n,\ D_B\frac{\partial C}{\partial y} + \frac{D_T}{T_\infty}\frac{\partial T}{\partial y} = 0,\ \ at\ y = 0.$$

$$u \to 0, \qquad T \to T_\infty, \qquad C \to C_\infty, \qquad at\ \ y \to \infty. \tag{6}$$

Where, $a > 0$ is for the stretching channel walls.

The Roseland approximation of the radiative heat flux is arranged by

$$q_r = \frac{-4\sigma^*}{3k^*}\frac{\partial T^4}{\partial y}, \tag{7}$$

Here T^4 as a linear relation of temperature via Taylor's sequence expansion about T_∞ and ignoring advanced terms, thus

$$T^4 \approx 4{T_\infty}^3 T - {T_\infty}^4. \tag{8}$$

In view of the similarity transformation

$$u = ax^n f'(\eta), \qquad v = -ax^{(n-1)/2}\sqrt{\frac{\nu}{a}}(\frac{n+1}{2}f(\eta) + \frac{n-1}{2}\eta f'(\eta)), \tag{9}$$

$$\eta = \sqrt{\frac{a}{\nu}}x^{(n-1)/2}y, \qquad \theta(\eta) = \frac{T - T_\infty}{T_w - T_\infty}, \qquad \phi(\eta) = \frac{C - C_\infty}{C_w - C_\infty}. \tag{10}$$

With (7)-(10), equations (2)-(6)are reduced to the next arrangement.

$$(1+\frac{1}{\beta})f'''-n(f')^2+(\frac{n+1}{2})ff''-Mnf'+k_2f'+G_T\theta+G_C\phi=0, \tag{11}$$

$$((1+Nr)/Pr)\theta''-nf'\theta+(\frac{n+1}{2})f\theta'+Nb\theta'\phi'+Nt(\theta')^2+(1+\frac{1}{\beta})Ec(f'')^2$$
$$+Q\theta+MnEc(f')^2+Du\phi''=0, \tag{12}$$

$$\phi''+(\frac{n+1}{2})Scf\phi'+\frac{Nt}{Nb}\theta''-ScK\phi=0. \tag{13}$$

With limit circumstances

$$f(0)=f_w,\quad f'(0)=1,\quad \theta(0)=1,\quad Nb\phi'(0)+Nt\theta'(0)=0,\quad at\ \ \eta=0. \tag{14a}$$

$$f'(\infty)\to 0,\quad \theta(\infty)\to 0,\quad \phi(\infty)\to 0,\quad at\ \ \eta\to\infty. \tag{14b}$$

Where, $Mn=\frac{\sigma B^2(x)}{\rho a x^{n-1}}$ shows the magnetic parameter, $k_2=\frac{\nu}{k' a x^{n-1}}$ indicates the permeability parameter, $G_T=\frac{g_0\beta_T(T_w-T_\infty)}{a^2x^{2n-1}}$ and $G_C=\frac{g_0\beta_C(C_w-C_\infty)}{a^2x^{2n-1}}$ indicate the local temperature and concentration Grashof number respectively, $Pr=\frac{\nu}{\alpha}$ shows the Prandtl number, $Q=\frac{Q_0}{\rho a c_p x^{n-1}}$ indicates the heat generation or absorption, $Nr=\frac{16\sigma^* {T_\infty}^3}{3kk^*}$ directs the radiation parameter, $Ec=\frac{u_w^2}{c_p(T_w-T_\infty)}$ shows the Eckert number, $Nb=\frac{\tau D_B(C_w-C_\infty)}{\nu}$ directs the Brownian motion parameter, $Nt=\frac{\tau D_T(T_w-T_\infty)}{\nu T_\infty}$ indicates the thermophoresis diffusion influence, $Du=\frac{D_BK_T(C_w-C_\infty)}{c_sc_p\nu(T_w-T_\infty)}$ specifies the Dufour number, $Sc=\frac{\nu}{D_B}$ directs the Schmidt number, $K=\frac{k_1}{ax^{n-1}}$ shows the chemical reaction parameter, and $f_w=\frac{-2v_w}{(n+1)\sqrt{\nu a x^{n-1}}}$ indicates the suction or blowing parameter.

Physical Quantities:

Skin Friction Coefficient(C_{fx})**:** The skin friction coefficient is known as follows:

$$C_{fx}=\frac{\tau_w}{\rho u_w^2},\ \ where\ \ \tau_w=\mu_B(1+\frac{1}{\beta})(\frac{\partial u}{\partial y})_{y=0}. \tag{15}$$

Heat Transfer Coefficient: The non-dimensional Nusselt number (Nu_x) is given by

$$Nu_x=\frac{xq_w}{k(T_w-T_\infty)},\ \ where\ \ q_w=-k(\frac{\partial T}{\partial y})_{y=0}. \tag{16}$$

Mass Transfer Coefficient: The rate of mass transfer is derived by a Sherwood number (Sh_x) which is given by

$$Sh_x=\frac{xm_w}{D_B(C_w-C_\infty)},\ \ where\ \ m_w=-D_B(\frac{\partial C}{\partial y})_{y=0}. \tag{17}$$

After solving the equation (15), (16) and (17) with equation (9) and (10), we gain

drag force

$${Re_x}^{1/2}C_{fx}=(1+\frac{1}{\beta})f''(0),$$

local Nusselt

$${Re_x}^{1/2}Nu_x=-\theta'(0),$$

local Sherwood

$$Re_x{}^{1/2}Sh_x = -\phi'(0). \tag{18}$$

Where,τ_w indicates the wall shear stress, k signifies the thermo nano-fluid conductivity, q_w shows the surface heat flux, and m_w directs the surface mass flux, $Re_x = \frac{u_w x}{\nu}$ shows the local Reynolds number.

We explain the reduces equations (11)-(13) with limitations (14a) and (14b) using Runge -Kutta fourth-order method along with shooting technique.

3 Results and Discussion:

The impacts of the numerous types of non-dimensional parameters values to have a physical considerate of the work like, the magneto impact Mn, f_w (suction or blowing), β Casson parameter, heat source or sink impact Q, Dufour impact Du, Brownian diffusivity Nb, Eckert parameter Ec, thermophoresis diffusivity Nt, radiative impact Nr, Prandtl effect Pr, Schmidt impact Sc, chemically reactive influence K, permeability influence k_2, Grashof number impact (G_T *and* G_C), and power law index n, over the momentum graphs $f'(\eta)$, temperature graphs $\theta(\eta)$, and concentration graphs $\phi(\eta)$ discussed through graphs [Figure 2 - Figure 23] and tables along with the influence of drag force $Re_x{}^{1/2}C_{fx}$, local Nusselt $Re_x{}^{1/2}Nu_x$ local Sherwood $Re_x{}^{1/2}Sh_x$. Non-dimensional equations (11)-(13) with limitations (14a) and (14b) solved by Runge- Kutta fourth-order method with shooting technique. After we find the values of heat transfer and mass transfer and draw the graph by MATLAB software. Consider the values of parameters $n = 3$ *or* $1, \beta = 0.1$ *or* $1, Mn = 0.1, k_2 = 0.1, Pr = 0.1, Q = 0.1, Nr = 0.1, Sc = 0.1, K = 0.1, G_T = 0.1, G_C = 0.1, Ec = 0.1, Du = 0.1, Nb = 0.1, Nr = 0.1, f_w = 0.1$.

The influence of the Casson nanofluid parameterβ on the momentum profile with power law index $n = 3$ and 1 is seen in [Figure 2] . The momentum graph drops as β increases in both situations of n, owing to the upsurge in plastic dynamic viscosity, which produces hindrance in the fluid flow. When $n = 3$, the momentum of the Casson nanofluid is greater than that of the Casson nanofluid when $n = 1$. With the track erect to the x-axis, [Figure 3] displays the lowering momentum impact of increased magnetic number Mn owing to the solid Lorentz force, which generates greater resistance in the fluid flow in both situations of Casson fluid $\beta = 0.1$ and 1. [Figure 4] depicts the failure velocity with suction or blowing parameter f_w due to nanofluid heat and thermolayer thickness for $n = 3$ and $n = 1$. When the permeability parameter k_2 rises to $\beta = 0.1$ and 1, the momentum decreases as seen in [Figure 5]. The momentum upsurges due to a rise in buoyant force with growing values of local concentration Grashof number G_C and local temperature Grashof number G_T, in [Figure 6] and [Figure 7] for $\beta = 0.1$ and 1, respectively.

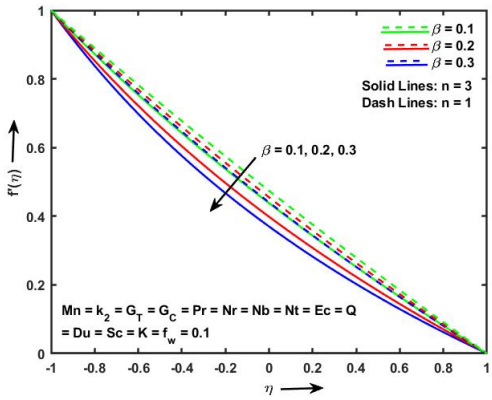

Figure 2: Velocity display of Casson fluid parameter β.

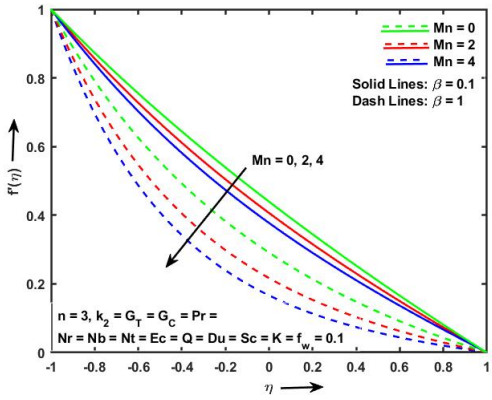

Figure 3: Velocity display of Magnetic parameter Mn.

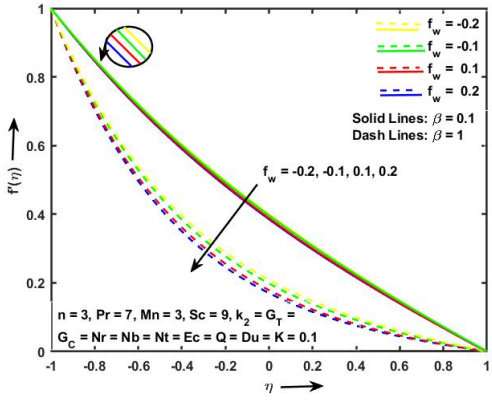

Figure 4: Velocity display of parameter f_w.

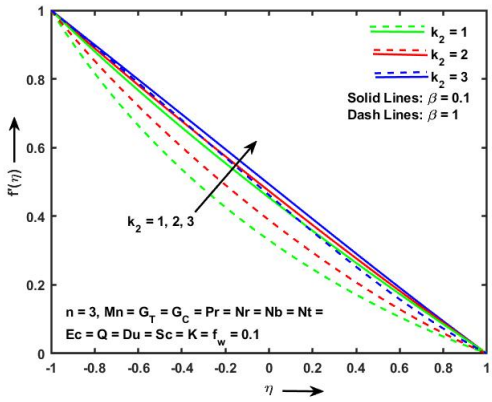

Figure 5: Velocity display of parameter k_2.

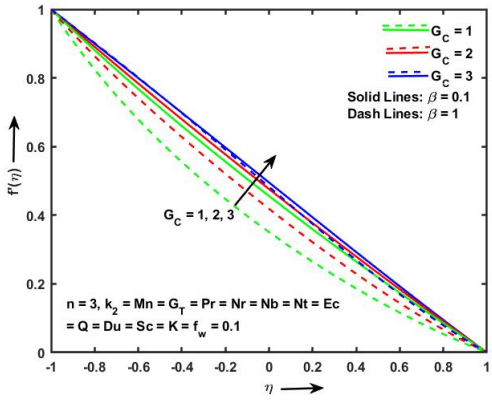

Figure 6: Velocity display of parameter G_C.

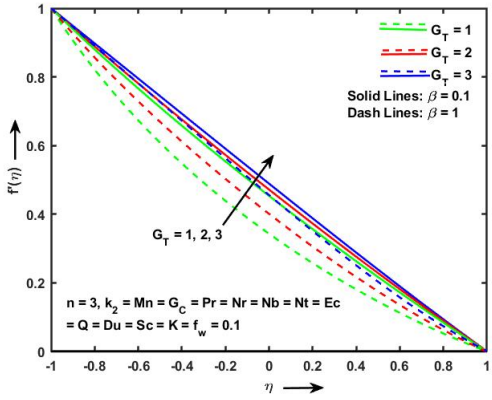

Figure 7: Velocity display of parameter G_T.

[Figure 8] illustrations the result of increasing the Dufour number on temperature between $\beta = 0.1$ and 1. [Figure 9] depicts the increasing influence of temperature on Eckert number Ec. The temperature rise as a result of the viscous dissipative term, which generates heat as a result of frictional heating between the fluid constituents. This additional heat resulted in a rise in temperature, which was connected to an increase in boundary layer breadth. [Figure 10] shows how temperature rises when the radiation parameter Nr between $\beta = 0.1$ and 1 increases. The $k*$ (absorption coefficient) lowers when there is an ascendant in Nr. An increase in f_w falloffs the nanofluid heat and thermolayer width owing to heated nanofluid pulled close to sheet is seen in [Figure 11]. As a result, in both scenarios of $\beta = 0.1$ and 1 with increase f_w, the temperature decreases. The Prandtl number Pr represents the ratio of momentum and thermal diffusivity. The temperature is lowered when Pr is increased (in [Figure 12]). Due to thermal layer thickness, [Figure 13] depicts the temperature increase with increasing heat production or absorption parameter Q (heat create in fluid for $Q > 0$ and heat absolve in fluid for $Q < 0$).

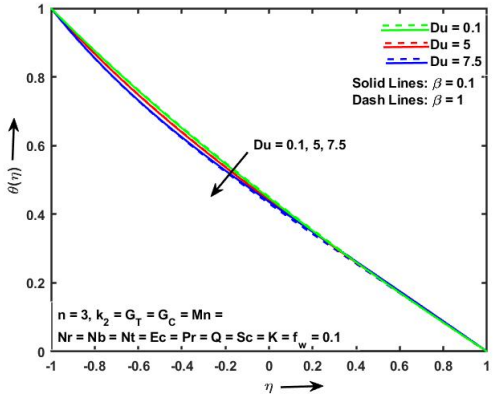

Figure 8: Temperature display of parameter Du,

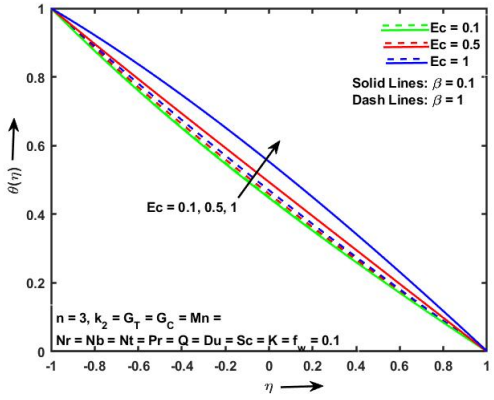

Figure 9: Temperature display of parameter Ec.

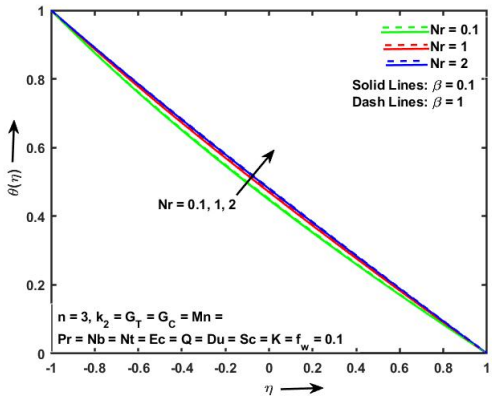

Figure 10: Temperature display of parameter Nr.

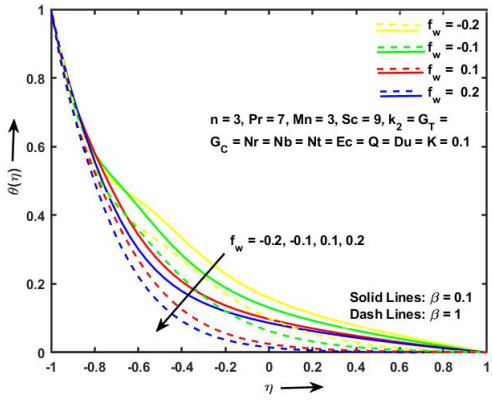

Figure 11: Temperature display of parameter f_w.

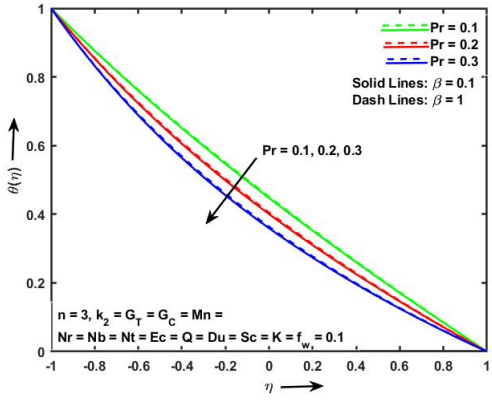

Figure 12: Temperature display of parameter Pr.

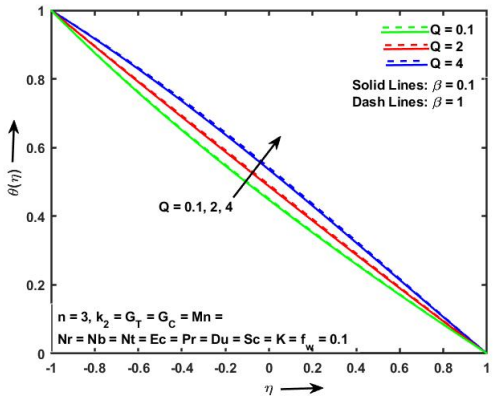

Figure 13: Temperature display of parameter Q.

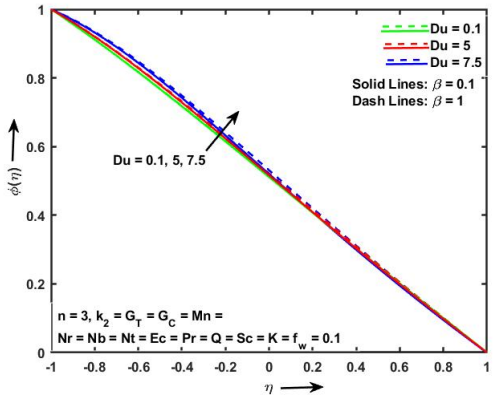

Figure 14: Concentration display of parameter Du.

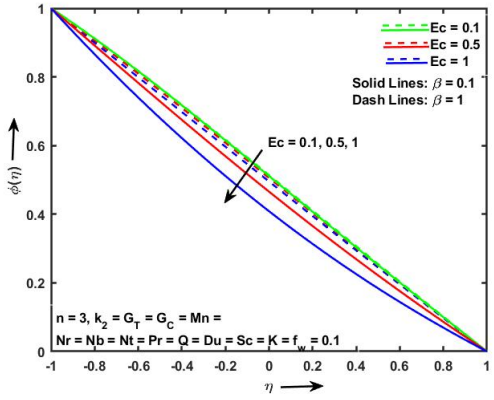

Figure 15: Concentration display of parameter Ec.

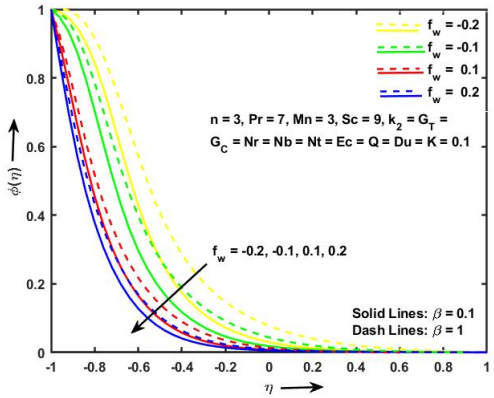

Figure 16: Concentration display of parameter f_w.

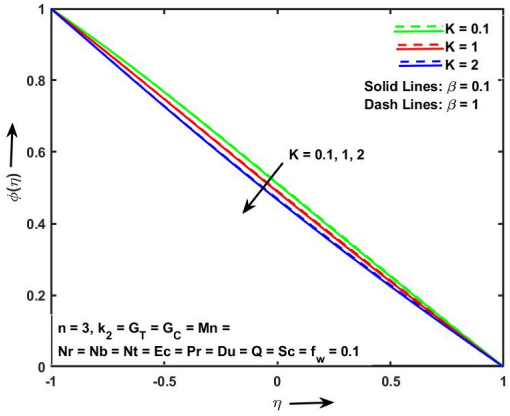

Figure 17: Concentration display of parameter K.

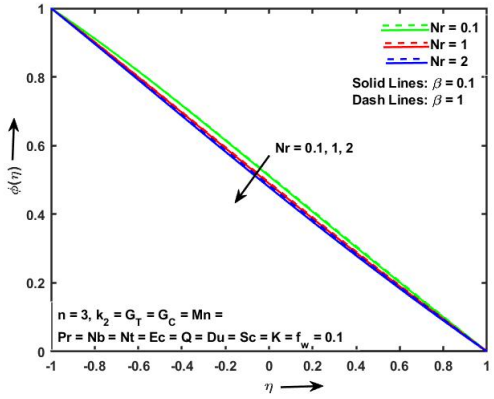

Figure 18: Concentration display of parameter Nr.

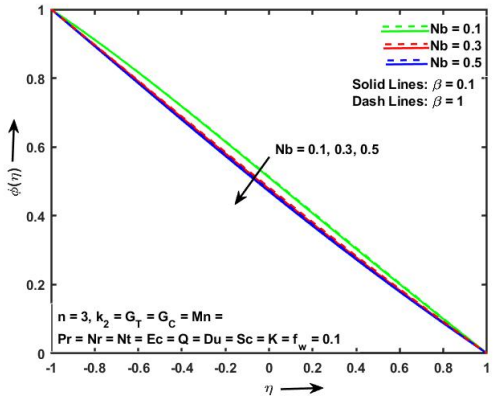

Figure 19: Concentration display of parameter Nb.

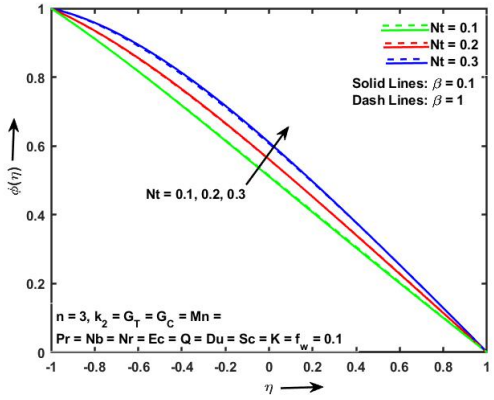

Figure 20: Concentration display of parameter Nt.

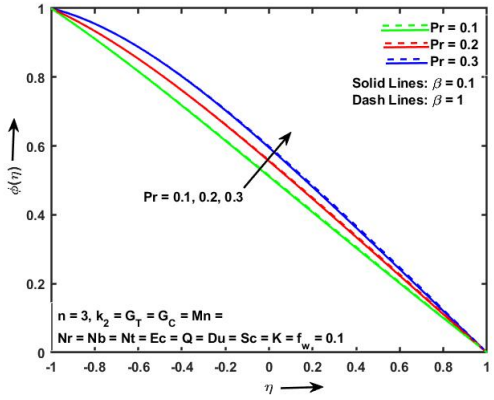

Figure 21: Concentration display of parameter Pr.

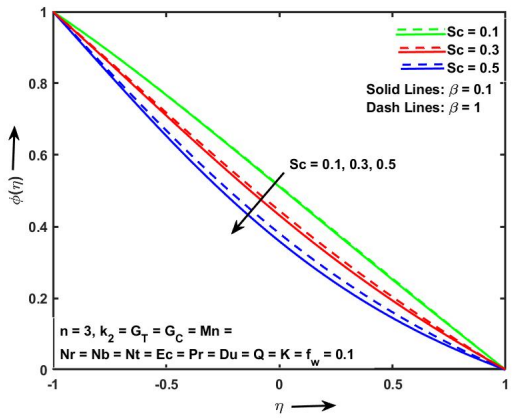

Figure 22: Concentration display of parameter Sc.

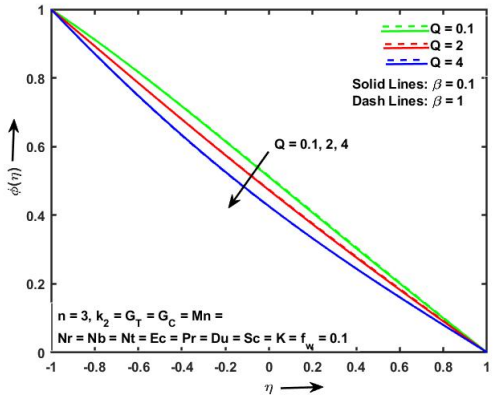

Figure 23: Concentration display of parameter Q.

[Figure 14] depicts an increment of concentration shape with growing Dufour number Du. [Figure 15]-[Figure 19] show the decay volume fraction graph for both $\beta = 0.1$ and 1 of Eckert parameter Ec, suction or blowing impact f_w, chemically reactive imapct K, and radiation parameter Nr. [Figure 20] describes the falling impact of concentration profile of upsurge Brownian parameter Nb for both $\beta = 0.1$ and 1. Similarly, impact of decay volume fraction of increase thermo-diffusion influence showing in [Figure 20]. [Figure 21] shows the effect of rise Prandtl number Pr on growing concentration profile for both $\beta = 0.1$ and 1. Increasing Schmidt number Sc and heat generation and absorption parameter Q impact with declines volume fraction influence explains in [Figure 22] and [Figure 23] respectively.

Table I: Numerical result of drag force coefficient, Nusselt number Nu, and Sherwood number of numerous parameters when $\beta = 0.1$ and 1 and $n = 3$.

Mn	k_2	G_T	G_C	f_w	Pr	Nr	Nb	Nt	Ec	Q	Du	Sc	K	$f''(0)$	$\theta'(0)$	$\phi'(0)$
0 2 4	0.1	0.1	0.1	0.1	0.1	0.1	0.1	0.1	0.1	0.1	0.1	0.1	0.1	-0.6589 -0.7599 -0.8538 -1.1769 -1.5325 -1.8312	-0.6429 -0.6269 -0.6119 -0.6389 -0.6179 -0.6009	-0.4222 -0.4360 -0.4492 -0.4182 -0.4352 -0.4492
0.1	1 2 3	0.1	0.1	0.1	0.1	0.1	0.1	0.1	0.1	0.1	0.1	0.1	0.1	-0.6159 -0.5609 -0.5309 -1.0129 -0.7849 -0.5249	-0.6459 -0.6499 -0.6549 -0.6469 -0.6579 -0.6719	-0.4192 -0.4162 -0.4122 -0.4122 -0.4032 -0.3942
0.1	0.1	1 2 3	0.1	0.1	0.1	0.1	0.1	0.1	0.1	0.1	0.1	0.1	0.1	-0.6169 -0.5639 -0.5119 -0.9879 -0.7638 -0.5458	-0.6459 -0.6499 -0.6539 -0.6489 -0.6599 -0.6699	-0.4192 -0.4162 -0.4132 -0.4102 -0.4022 -0.3952
0.1	0.1	0.1	1 2 3	0.1	0.1	0.1	0.1	0.1	0.1	0.1	0.1	0.1	0.1	-0.6129 -0.5559 -0.4999 -0.9723 -0.7287 -0.4903	-0.6459 -0.6509 -0.6549 -0.6499 -0.6629 -0.6739	-0.4192 -0.4152 -0.4122 -0.4092 -0.4002 -0.3922
3	0.1	0.1	0.1	-0.2 -0.1 0.1 0.2	7	0.1	0.1	0.1	0.1	0.1	0.1	9	0.1	-0.785275 -0.794275 -0.8139 -0.8229 -1.5580 -1.6079 -1.7109 -1.7639	-2.792727 -3.240827 -3.4749 -3.1099 -2.90922 -3.4316 -3.9492 -3.7849	-0.107859 -0.389959 -2.2192 -3.8882 0.11995 -0.0675 -1.5985 -3.0582

0.1	0.1	0.1	0.1	0.1	0.1 0.2 0.3	0.1	0.1	0.1	0.1	0.1	0.1	0.1	0.1	-0.6639 -0.6639 -0.6639 -1.1969 -1.1969 -1.1969	-0.6419 -0.7779 -0.9079 -0.6379 -0.7729 -0.9039	-0.4222 -0.2868 -0.1568 -0.4188 -0.2838 -0.1518
0.1	0.1	0.1	0.1	0.1	0.1	0.1 1 2	0.1	0.1	0.1	0.1	0.1	0.1	0.1	-0.6639 -0.6639 -0.6639 -1.1969 -1.1969 -1.1969	-0.6419 -0.5789 -0.5529 -0.6379 -0.5765 -0.5505	-0.4222 -0.4852 -0.5122 -0.4188 -0.4808 -0.5058
0.1	0.1	0.1	0.1	0.1	0.1	0.1	0.1 0.3 0.5	0.1	0.1	0.1	0.1	0.1	0.1	-0.6639 -0.6639 -0.6639 -1.1971 -1.1977 -1.1977	-0.6419 -0.6479 -0.6539 -0.6379 -0.6439 -0.6499	-0.4222 -0.5152 -0.5342 -0.4188 -0.5092 -0.5272
0.1	0.1	0.1	0.1	0.1	0.1	0.1	0.1	0.1 0.2 0.3	0.1	0.1	0.1	0.1	0.1	-0.6639 -0.6639 -0.6635 -1.1971 -1.1955 -1.1945	-0.6419 -0.6409 -0.6399 -0.6379 -0.6369 -0.6359	-0.4222 -0.2822 -0.1442 -0.4188 -0.2828 -0.1482
0.1	0.1	0.1	0.1	0.1	0.1	0.1	0.1	0.1	0.1 0.5 1	0.1	0.1	0.1	0.1	-0.6639 -0.6636 -0.6636 -1.1971 -1.1971 -1.1971	-0.6419 -0.5239 -0.3749 -0.6379 -0.6009 -0.5549	-0.4222 -0.5412 -0.6902 -0.4188 -0.4558 -0.5018
0.1	0.1	0.1	0.1	0.1	0.1	0.1	0.1	0.1	0.1	0.1 2 4	0.1	0.1	0.1	-0.6639 -0.6639 -0.6639 -1.1971 -1.1971 -1.1971	-0.6419 -0.5309 -0.4019 -0.6379 -0.5249 -0.3939	-0.4222 -0.5337 -0.6627 -0.4188 -0.5318 -0.6638
0.1	0.1	0.1	0.1	0.1	0.1	0.1	0.1	0.1	0.1	0.1	0.1 5 7.5	0.1	0.1	-0.6639 -0.6639 -0.6639 -1.1971 -1.1971 -1.1971	-0.6419 -0.7019 -0.7899 -0.6379 -0.7019 -0.7979	-0.4222 -0.3632 -0.2762 -0.4188 -0.3558 -0.2602

														-0.6639	**-0.6419**	**-0.4222**
														-0.6636	**-0.6409**	**-0.5572**
												0.1		**-0.6642**	**-0.6389**	**-0.6972**
0.1	**0.1**	**0.1**	**0.1**	**0.1**	**0.1**	**0.1**	**0.1**	**0.1**	**0.1**	**0.1**	**0.1**	**0.3**	**0.1**			
												0.5		**-1.1971**	**-0.6379**	**-0.4188**
														-1.1979	**-0.6369**	**-0.5388**
														-1.1999	**-0.6349**	**-0.6628**
														-0.6639	**-0.6419**	**-0.4222**
														-0.6639	**-0.6409**	**-0.4832**
													0.1	**-0.6639**	**-0.6409**	**-0.5472**
0.1	**0.1**	**0.1**	**0.1**	**0.1**	**0.1**	**0.1**	**0.1**	**0.1**	**0.1**	**0.1**	**0.1**	**0.1**	**1**			
													2	**-1.1971**	**-0.6379**	**-0.4188**
														-1.1971	**-0.6369**	**-0.4798**
														-1.1981	**-0.6369**	**-0.5438**

Table II: Mathematical outcome of drag force coefficient, Nusselt number Nu, and Sherwood number of Casson nanofluid parameter β when $n = 3$.

β	Mn	k_2	G_T	G_C	f_w	Pr	Nr	Nb	Nt	Ec	Q	Du	Sc	K	$f^{''}(0)$	$\theta'(0)$	$\phi'(0)$
															-0.5589	**-0.5389**	**-0.4982**
															-0.6049	**-0.5489**	**-0.4872**
0.1															**-0.6419**	**-0.5519**	**-0.4842**
0.2	**0.1**	**0.1**	**0.1**	**0.1**	**0.1**	**0.1**	**0.1**	**0.1**	**0.1**	**0.1**	**0.1**	**0.1**	**0.1**	**0.1**			
0.3															**-0.6639**	**-0.6419**	**-0.4222**
															-0.7819	**-0.6469**	**-0.4152**
															-0.8732	**-0.6469**	**-0.4142**

4 Conclusion:

The impact of hydromagnetic Casson nanofluid's boundary layer on a nonlinear stretching sheet in 2D with the impact of viscid dissipative impact, Dufour number Du, heat absorption or generation Q impact, and suction or blowing impact, among other things, is examined mathematically. The skinfriction coefficient grows as permeability and Grashof number increase. As the Dufour number improves, the Nusselt number drops, whereas the Sherwood number drops as the chemical reactive impression improves. The Runge Kutta 4^{th} order procedure, as well as the shooting technique and MATLAB software, are used to arrive at the mathematical answer. The following are some of the study's key findings:

- Momentum display decreases when β, Mn, and f_w rise, but increases as k_2, G_T, and G_C rise.
- The temperature graph decreases when Du, f_w, and Pr increase, and increases as Ec, Nr, and Q increase.
- The volume fraction distribution improved when Du, Nt, Pr increased and falloffs in Ec, f_w, K, Nr, Nb, Sc, and Q decreased.
- The skin friction coefficient decreases when Mn, Nr, f_w, Nb, Ec, Q, Sc, K increases, while it climbs as k_2, G_T, G_C, β, Pr, Nt, and Du increase.
- The Nusselt number increases as Mn, Nr, Nt, Ec, Q, Sc, and K levels rise, but decreases as k_2, G_T, G_C, β, f_w, Pr, Nb, and Du levels rise.
- The Sherwood number increased when k_2, G_T, G_C, and Nt increased, but decreased as Mn, β, f_w, Nb, Sc, and K increased.

References

[1] AC Venkata Ramudu, K Anantha Kumar, V Sugunamma, and N Sandeep. Impact of soret and dufour on mhd casson fluid flow past a stretching surface with convective–diffusive conditions. *Journal of Thermal Analysis and Calorimetry*, pages 1–11, 2021.

[2] Adnan Saeed Butt, Khadija Maqbool, Syed Muhammad Imran, and Babar Ahmad. Entropy generation effects in mhd casson nanofluid past a permeable stretching surface. *International Journal of Exergy*, 31(2):150–171, 2020.

[3] Ahmed A Afify. The influence of slip boundary condition on casson nanofluid flow over a stretching sheet in the presence of viscous dissipation and chemical reaction. *Mathematical Problems in Engineering*, 2017, 2017.

[4] Ahmed F Al-Hossainy, Mohamed R Eid, and Mohamed Sh Zoromba. Sqlm for external yield stress effect on 3d mhd nanofluid flow in a porous medium. *Physica Scripta*, 94(10):105208, 2019.

[5] Anwar Saeed, Poom Kumam, Saleem Nasir, Taza Gul, and Wiyada Kumam. Non-linear convective flow of the thin film nanofluid over an inclined stretching surface. *Scientific Reports*, 11(1):1–15, 2021.

[6] Asifa Tassaddiq, Ilyas Khan, Kottakkaran Sooppy Nisar, and Jagdev Singh. Mhd flow of a generalized casson fluid with newtonian heating: A fractional model with mittag–leffler memory. *Alexandria Engineering Journal*, 59(5):3049–3059, 2020.

[7] Ayesha Siddiqui and Bandari Shankar. Mhd flow and heat transfer of casson nanofluid through a porous media over a stretching sheet. In *Nanofluid Flow in Porous Media*. IntechOpen, 2019.

[8] Faraz Faraz, Sajjad Haider, and Syed Muhammad Imran. Study of magnetohydrodynamics (mhd) impacts on an axisymmetric casson nanofluid flow and heat transfer over unsteady radially stretching sheet. *SN Applied Sciences*, 2(1):1–17, 2020.

[9] Fekry M Hady, Fouad S Ibrahim, Sahar M Abdel-Gaied, and Mohamed R Eid. Radiation effect on viscous flow of a nanofluid and heat transfer over a nonlinearly stretching sheet. *Nanoscale Research Letters*, 7(1):1–13, 2012.

[10] G Mahanta and S Shaw. 3d casson fluid flow past a porous linearly stretching sheet with convective boundary condition. *Alexandria Engineering Journal*, 54(3):653–659, 2015.

[11] G Sarojamma and K Vendabai. Boundary layer flow of a casson nanofluid past a vertical exponentially stretching cylinder in the presence of a transverse magnetic field with internal heat generation/absorption. *International Journal of Mathematical and Computational Sciences*, 9(1):138–143, 2015.

[12] Hammad Alotaibi, Saeed Althubiti, Mohamed R Eid, and KL Mahny. Numerical treatment of mhd flow of casson nanofluid via convectively heated nonlinear extending surface with viscous dissipation and suction/injection effects. *Computers, Materials & Continua*, 66(1):229–245, 2020.

[13] Ibukun Sarah Oyelakin, Sabyasachi Mondal, and Precious Sibanda. Unsteady casson nanofluid flow over a stretching sheet with thermal radiation, convective and slip boundary conditions. *Alexandria engineering journal*, 55(2):1025–1035, 2016.

[14] Imran Ullah, Krishnendu Bhattacharyya, Sharidan Shafie, and Ilyas Khan. Unsteady mhd mixed convection slip flow of casson fluid over nonlinearly stretching sheet embedded in a porous medium with chemical reaction, thermal radiation, heat generation/absorption and convective boundary conditions. *PloS one*, 11(10):e0165348, 2016.

[15] Jagdev Singh, Devendra Kumar, and Sunil Kumar. An efficient computational method for local fractional transport equation occurring in fractal porous media. *Computational and Applied Mathematics*, 39(3):1–10, 2020.

[16] Kushal Dhar Dwivedi and Jagdev Singh. Numerical solution of two-dimensional fractional-order reaction advection sub-diffusion equation with finite-difference fibonacci collocation method. *Mathematics and Computers in Simulation*, 181:38–50, 2021.

[17] Maria Imtiaz, Tasawar Hayat, and Ahmed Alsaedi. Mixed convection flow of casson nanofluid over a stretching cylinder with convective boundary conditions. *Advanced Powder Technology*, 27(5):2245–2256, 2016.

[18] Mohamed R Eid and Kasseb L Mahny. Flow and heat transfer in a porous medium saturated with a sisko nanofluid over a nonlinearly stretching sheet with heat generation/absorption. *Heat Transfer—Asian Research*, 47(1):54–71, 2018.

[19] Mohamed R Eid. Chemical reaction effect on mhd boundary-layer flow of two-phase nanofluid model over an exponentially stretching sheet with a heat generation. *Journal of Molecular Liquids*, 220:718–725, 2016.

[20] Mohamed R Eid, KL Mahny, Amanullah Dar, and Taseer Muhammad. Numerical study for carreau nanofluid flow over a convectively heated nonlinear stretching surface with chemically reactive species. *Physica A: Statistical Mechanics and its Applications*, 540:123063, 2020.

[21] Mohamed R Eid. Time-dependent flow of water-nps over a stretching sheet in a saturated porous medium in the stagnation-point region in the presence of chemical reaction. *Journal of Nanofluids*, 6(3):550–557, 2017.

[22] M Mustafa and Junaid Ahmad Khan. Model for flow of casson nanofluid past a non-linearly stretching sheet considering magnetic field effects. *AIP advances*, 5(7):077148, 2015.

[23] M Wahiduzzaman, Md Musa Miah, Md Babul Hossain, Fatematuz Johora, and Shamol Mistri. Mhd casson fluid flow past a non-isothermal porous linearly stretching sheet. *Prog. Nonlinear Dynamics Chaos*, 2(2):61–69, 2014.

[24] Nargis Khan, Iram Riaz, Muhammad Sadiq Hashmi, Saed A Musmar, Sami Ullah Khan, Zahra Abdelmalek, and Iskander Tlili. Aspects of chemical entropy generation in flow of casson nanofluid between radiative stretching disks. *Entropy*, 22(5):495, 2020.

[25] Prabhakar Besthapu, Shanker Bandari, et al. Mixed convection mhd flow of a casson nanofluid over a nonlinear permeable stretching sheet with viscous dissipation. *Journal of Applied Mathematics and Physics*, 3(12):1580, 2015.

[26] S Pramanik. Casson fluid flow and heat transfer past an exponentially porous stretching surface in presence of thermal radiation. *Ain Shams Engineering Journal*, 5(1):205–212, 2014.

[27] P Bala Anki Reddy. Magnetohydrodynamic flow of a casson fluid over an exponentially inclined permeable stretching surface with thermal radiation and chemical reaction. *Ain Shams Engineering Journal*, 7(2):593–602, 2016.

[28] R Vijayaragavan. Magnetohydrodynamic radiative casson fluid flow over a stretching sheet with heat source/sink. *Advances in Physics Theories and Applications*, 55:13–23, 2016.

[29] Sami Ul Haq, Saeed Ullah Jan, Syed Inayat Ali Shah, Ilyas Khan, and Jagdev Singh. Heat and mass transfer of fractional second grade fluid with slippage and ramped wall temperature using caputo-fabrizio fractional derivative approach. *AIMS Mathematics*, 5(4):3056–3088, 2020.

[30] Sihem Lahmar, Mohamed Kezzar, Mohamed R Eid, and Mohamed Rafik Sari. Heat transfer of squeezing unsteady nanofluid flow under the effects of an inclined magnetic field and variable thermal conductivity. *Physica A: Statistical Mechanics and Its Applications*, 540:123138, 2020.

[31] Sohail Nadeem, Rizwan Ul Haq, Noreen Sher Akbar, and Zafar Hayat Khan. Mhd three-dimensional casson fluid flow past a porous linearly stretching sheet. *Alexandria Engineering Journal*, 52(4):577–582, 2013.

[32] SA Shehzad, T Hayat, M Qasim, and S Asghar. Effects of mass transfer on mhd flow of casson fluid with chemical reaction and suction. *Brazilian Journal of Chemical Engineering*, 30(1):187–195, 2013.

[33] SM Abo-Dahab, MA Abdelhafez, Fateh Mebarek-Oudina, and SM Bilal. Mhd casson nanofluid flow over nonlinearly heated porous medium in presence of extending surface effect with suction/injection. *Indian Journal of Physics*, pages 1–15, 2021.

[34] SM Ibrahim, G Lorenzini, P Vijaya Kumar, and CSK Raju. Influence of chemical reaction and heat source on dissipative mhd mixed convection flow of a casson nanofluid over a nonlinear permeable stretching sheet. *International Journal of Heat and Mass Transfer*, 111:346–355, 2017.

[35] T Hayat, SA Shehzad, A Alsaedi, and MS Alhothuali. Mixed convection stagnation point flow of casson fluid with convective boundary conditions. *Chinese Physics Letters*, 29(11):114704, 2012.

[36] V Puneeth, S Manjunatha, JK Madhukesh, and GK Ramesh. Three dimensional mixed convection flow of hybrid casson nanofluid past a non-linear stretching surface: A modified buongiorno's model aspects. *Chaos, Solitons & Fractals*, 152:111428, 2021.

[37] Wasim Jamshed, Vivek Kumar, and Vikash Kumar. Computational examination of casson nanofluid due to a non-linear stretching sheet subjected to particle shape factor: Tiwari and das model. *Numerical Methods for Partial Differential Equations*, 2020.

[38] Zahir Shah, Poom Kumam, and Wejdan Deebani. Radiative mhd casson nanofluid flow with activation energy and chemical reaction over past nonlinearly stretching surface through entropy generation. *Scientific Reports*, 10(1):1–14, 2020.